

Are all RR Lyrae stars modulated?

Geza Kovacs¹

Konkoly Observatory of the Hungarian Academy of Sciences, Budapest, 1121 Konkoly Thege ut. 13-15, Hungary
e-mail: kovacs@konkoly.hu

Received 6 April 2018 / Accepted xx, xx 2018

ABSTRACT

We analyzed 151 variables previously classified as fundamental mode RR Lyrae stars from Campaigns 01 – 04 of the *Kepler* two wheel (K2) archive. By employing a method based on the application of systematics filtering with the aid of co-trending light curves in the presence of the large amplitude signal component, we searched for additional Fourier signals in the close neighborhood of the fundamental period. We found only 13 stars without such components, yielding the highest rate of 91% of modulated (Blazhko) stars detected so far. A detection efficiency test suggests that this occurrence rate likely implies a 100% underlying rate. Furthermore, the same test performed on a subset of the Large Magellanic Cloud RR Lyrae stars from the MACHO archive shows that the conjecture of high true occurrence rate fits well to the low observed rate derived from this database.

Key words. Stars: variables: RR Lyrae – Methods: data analysis

1. Introduction

Although RR Lyrae stars are among the most important objects for tracing galaxy structure and chemistry and thought to pulsate in the simplest way we can model by and large already from the mid sixties (Christy 1964), it is highly disturbing that when it goes to a more detailed modelling (e.g., steady multi-mode pulsation), our current (admittedly simple) models fail in a major way. Particular to these stars is the (quasi)periodic amplitude/phase change, commonly known as Blazhko phenomenon (Blazhko 1907, see also Shapley 1916). Most of the progress made in this issue comes from the side of the observations, largely attributed to the space missions *CoRoT* and *Kepler* (e.g., Benkő et al. 2014), Szabó et al. 2014. Still, even these highly accurate data were unable to deliver a ground-breaking discovery that would inspire physically sound (and working) idea.¹

There are also contradictory figures on the mere occurrence rates of the Blazhko (hereafter BL) stars. These rates (for fundamental mode stars) range from $\sim 12\%$ to $\sim 50\%$ (see Kovacs 2016 and Smolec 2016 and references therein). Interestingly, the analysis of the high-precision space observations yield apparently quite similar rates to those derived from classical ground-based data (Benkő et al. 2014, Jurcsik et al. 2009).

This, and the apparent lack of the application of the modern methods of time series analysis in this field prompted us to examine the occurrence rates of the BL stars from a subset of the available space data. Even without knowing the underlying physical cause of the BL phenomenon, it is clear that this single number may help to distinguish between various ideas. For example, models based on the resonance between radial modes will likely face difficulties if amplitude/phase modulation is indeed as common as the present study shows.

¹ The only exception is perhaps the discovery of the alternation of the maxima in certain phases of the Blazhko cycle, that is currently attributed to a high-order resonance involving the fundamental mode – see Buchler & Kollath (2011) and Smolec (2016) for some critical comments.

2. Datasets and the method of analysis

In establishing a solid, but not too extensive dataset proper for this introductory work, we opted for the *Kepler* two-wheel (K2) survey. Unfortunately, there are not too many well-documented (star-by-star) RR Lyrae surveys available for this mission. However, the variability survey of Armstrong et al. (2016) of the data of Campaigns 0–4 has proven to be extensive enough, suitable for the purpose of this work. We have chosen not to include C0, because of the short observational time span devoted to this campaign in the early phase of K2. A few basic parameters of the datasets used are listed in Table 1. As this table shows, there are several miss-classifications in the original list. Nevertheless, the number of the remaining stars is large enough to use them as a statistically significant sample in assessing the occurrence rate of the BL phenomenon. There are some 4–5 stars belonging to the globular cluster M4 in C02, otherwise all the rest are apparently Galactic field/halo stars (many of them are rather faraway objects). See Fig. 1 for the distribution of the 237 targets analyzed in this paper over the *Kepler* field of view during the four campaigns.

Table 1. Summary of the datasets used in this paper

Field	N_{tot}	N_{RR}	Source
C01	21	11	IPAC/K2 ExoFOP
C02	76	45	IPAC/K2 ExoFOP
C03	73	62	IPAC/K2 K2 Targets
C04	67	33	IPAC/K2 K2 Targets

Notes:

N_{tot} stands for the total number of stars classified as RRab stars by Armstrong et al. (2016). N_{RR} is for the actual number of RRab stars. The time series data were downloaded for C01 and C02 from <https://exofop.ipac.caltech.edu/> (see Petigura et al. 2015) and for for C03 and C04 from <https://exoplanetarchive.ipac.caltech.edu/>

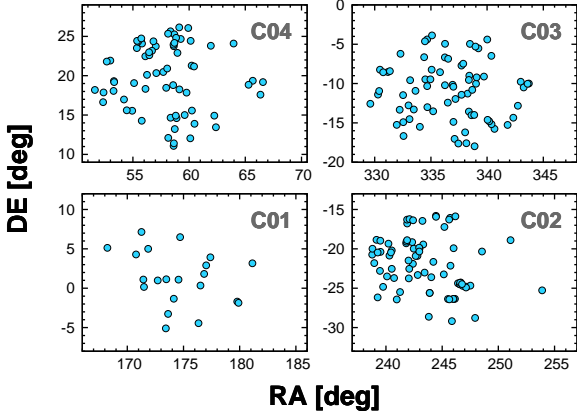


Fig. 1. Distribution of the stars analyzed in this paper (see Table 1) in the field of view of *Kepler*.

For fields C01 and C02, time series based on Simple Aperture Photometry (SAP) have been downloaded in ASCII format from the target inquiry page of the NASA Exoplanet Archive (IPAC). Field C03 and C04 time series data are not available at this site, but they are accessible through the ExoFOP link by the same host. To aid the method vital for filtering out instrumental systematics (TFA, Kovacs et al. 2005), in addition to the fundamental mode RR Lyrae (RRab) stars, 2–4 thousand stars were also downloaded for each field. These stars are distributed over the entire *Kepler* field of view and cover a wide range of brightness. All time series are of long cadence (i.e., with ~ 30 min sampling) and contain over 3000 data points with a continuous coverage of ~ 70 days.

It is well known that instrumental systematics are much more severe in the K2 phase of the *Kepler* mission than it was during the first phase with all four reaction wheels working. Therefore, correction for the various forms of systematics originating from this, and several other issues (e.g., ignition of thrusters) should be considered during the time series analysis. In the case of large amplitude variable stars this correction (if it is made without full modelling of the data) may lead to disastrous result. We guess that this is the main reason why variability studies, so far, largely avoided any filtering of systematics and tried to reach the best result with the aid of carefully chosen aperture forms and use only aperture photometry without any essential post-processing (e.g., Plachy et al. 2017).

To search for astronomical signals and tackle systematics at the same time, without deforming the signal, Foreman-Mackey et al. (2015) and Angus et al. (2016) employed full models, whereas Aigrain et al. (2016) developed a method based on the flexibility of modelling with Gaussian Process. As discussed by Kovacs et al. (2016), when these methods are used for period search for signals commensurable with the size of the systematics, due to the extra freedom introduced by the inclusion of the underlying (but unknown) signal, the resulting detection statistics becomes poorer than for the more standard methods, assuming no signal content (e.g., SysRem of Tamuz et al. 2005).

The situation is different when the period of the dominating signal is known and we search for small secondary signals hidden in the systematics. The very simple methodology one can follow has been touched upon in some of our earlier papers (Kovacs 2005, Kovacs & Bakos 2008). We described the method and illustrated its power through examples drawn from the K2

database in Kovacs (2018). For the sake of a more compact presentation, here we summarize the main steps of the analysis.

1. Choose N_{TFA} co-trending time series $\{U_j(i); j = 1, 2, \dots, N_{\text{TFA}}; i = 1, 2, \dots, N\}$ from the stars available in the field (interpolate – if needed – to bring the target and the co-trending time series to the same timebase). Note: in this study, we selected these stars from the bright end of the available stars, but no other selections were made (e.g., on the basis of variability).
2. Derive the fundamental frequency f_0 of the target $\{T(i); i = 1, 2, \dots, N\}$ from the SAP time series.
3. Compute the sine, cosine values up to the $N_{\text{FOUR}} - 1$ harmonics of f_0 : $\{S_j(i), C_j(i); j = 1, 2, \dots, N_{\text{FOUR}}; i = 1, 2, \dots, N\}$
4. Perform standard Least Squares minimization for a_0 , $\{a_j\}$ $\{b_k, c_k\}$ on the following expression:

$$\mathcal{D} = \sum_{i=1}^N [T(i) - F(i)]^2, \quad (1)$$

$$F(i) = a_0 + \sum_{j=1}^{N_{\text{TFA}}} a_j U_j(i) + \sum_{k=1}^{N_{\text{FOUR}}} b_k S_k(i) + c_k C_k(i). \quad (2)$$

5. Using the solution above, compute $T^{\hat{}}(i) = T(i) - a_0 - \sum_{j=1}^{N_{\text{TFA}}} a_j U_j(i)$ and find the new value of f_0 . Iterate on 3., 4. and 5., until convergence is reached.
6. With the converged f_0 , compute the residual $\{R(i) = T(i) - F(i); i = 1, 2, \dots, N\}$ and perform standard Fourier frequency analysis on $\{R(i)\}$ with pre-whitening.
7. After reaching the noise level, use all frequencies (f_0 and its harmonics, the new frequencies) and the co-trending time series to perform a grand fit according to step 4 (extended with the new frequencies).

We note that certain care must be taken at some steps of the analysis. For example, if the systematics are too large, then we need to perform a TFA analysis first, to derive a good estimate on f_0 (we had one such a case in the dataset analyzed). Also, some frequency proximity condition should be applied, otherwise the fit may become unstable. We found that requesting $|\Delta f| < 0.1/T$, where T is the total time span, yields stable fits.

3. Analysis, examples, observed occurrence rate

We analyzed all the 237 objects of Table 1 by using the method described in Sect. 2. A wide frequency band of $[0, 30]$ c/d was chosen to accommodate high harmonics. Even though the number of harmonics was high (14, throughout the analysis), in many cases leakage from the harmonics higher than the Nyquist frequency (24.47 c/d in the case of the present K2 data) caused a well-defined pattern from $\sim 10 - 15$ c/d. Our stoppage criterion for ending the pre-whitening cycle was $SNR < 6$, where $SNR = (A_{\text{peak}} - \langle A \rangle) / \sigma(A)$, with A denoting the amplitude spectrum with sigma-clipped average $\langle A \rangle$ and standard deviation $\sigma(A)$. The results presented in this paper are based on runs using 100 co-trending stars. We note that in the preliminary study we used 400 and we ended up with the same conclusion. In critical cases we used different number of co-trending light curves, to make sure that the final classification is robust enough.

We show two examples on the performance of the method used in this paper. Fig. 2 shows a case when the SAP data suffer from some well visible systematics. Our focus of interest is the light curve labelled by TFA(FOUR). This light curve obtained after subtracting the best combination of the co-trending

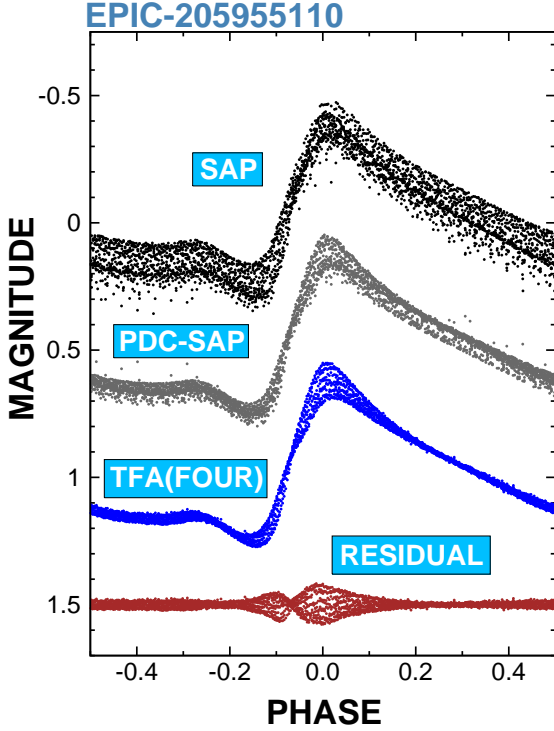


Fig. 2. An example from Campaign 3 on the performance of the filtering method used in this work in searching for secondary signal components. The light curves have been shifted vertically for better visibility. The lowermost light curve resulted from the subtraction of the large amplitude pulsation component (including the 14-th harmonics) from the systematics-filtered TFA(FOUR) light curve.

light curves from the SAP data (i.e., $TFA(FOUR) \rightarrow T(i) - a_0 - \sum_{j=1}^{N_{TFA}} a_j U_j(i)$, see Sect. 2). In principle, these data should contain only the modulated pulsation of the star. Indeed, the filtered light curve shows a very clean pattern of modulation. In comparison, it is also visible that although the standard *Kepler* pipeline (PDC-SAP, see Smith et al. 2012) helps to alleviate signal distortion at some degree, there are obvious remnants of systematics, leaving a less cleanly defined BL modulation on the filtered light curve.

In another example in Fig. 3 we show the rare case when the systematics are small. Here we expect the method leaving the SAP signal basically intact. A brief visual inspection shows that it is indeed the case for the TFA(FOUR) light curve, but the filtering method employing a Gaussian Process model (K2SC, see Agrain et al. 2016) apparently introduces additional noise in the data. These two examples show that employing a model best suited to the time series under scrutiny – in this case a periodic signal with a Fourier representation – greatly helps in the separation of systematics from the physically relevant signal content. Yet another important difference between our method and both of those mentioned above, is the high number of co-trending time series used by TFA. In this way we can handle a larger variety of systematics than relying only the leading PCA components, as in the case of the PDC pipeline.

The detection of the BL modulation is illustrated in Fig. 4. The upper panel shows the “easy” case: well-separated modula-

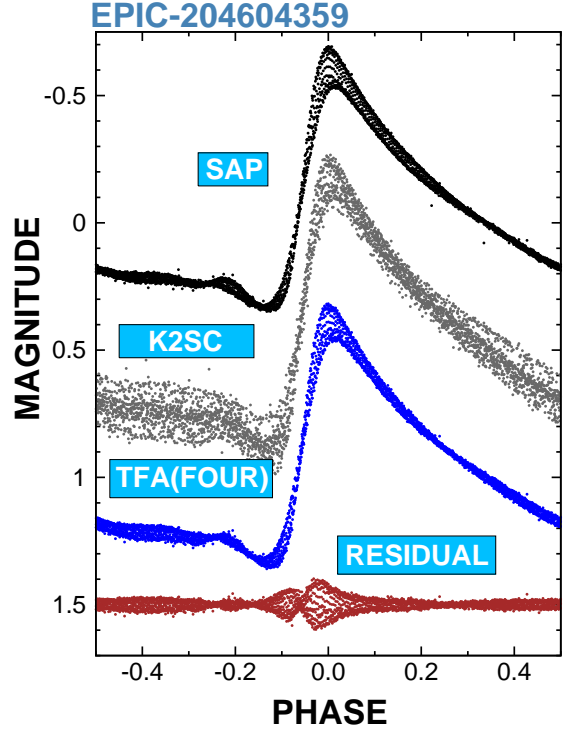


Fig. 3. An example from Campaign 2 on the performance of our method in the case of low level of systematics. For comparison, the signal processing method based on a very flexible Gaussian Process model (K2SC, Agrain et al. 2016), is also shown.

tion side lobes with high amplitudes. The lower panel shows one of the cases with jammed power content at the fundamental frequency. In these cases either the low modulation amplitude or the inherently complex nature of the modulation (or both) prevent a reliable estimation of the modulation period. Nevertheless, we classified also these cases as BL, since the significant power content at the fundamental frequency.

With multiple visual inspection of the frequency spectra of the 237 stars, we ended up with the following criterion for classifying a RRab stars as a BL star. *If at any stage of the pre-whitening cycle an excess of power occurs with $SNR > 6$ at a frequency f , satisfying $|f - f_0| < 0.1$ c/d, and this feature proves to be stable against changing the number of co-trending time series, then the star is classified as a BL star.* It is important to note that only about a dozen stars required deeper examinations in respect of this criterion. Once the side lobe/lobes is/are identified, two parameters were attached to the star to characterize its BL properties: a) maximum side lobe amplitude, $A_m = MAX\{A_i; i = 1, 2, \dots, N_s\}$, where $\{A_i\}$ are the side lobe amplitudes (altogether N_s of them), and b) the modulation frequency $f_m = f_0 - f(A_m)$. Please note that we selected these two parameters for the rough characterization of the BL stars, mainly to establish the distribution of A_m , which is directly connected to the issue of detectability, the focus of this work.

As we have already mentioned, we found only 151 stars from the original set of 237 stars that can be classified as RRab stars. With the criterion mentioned, 138 of them proved to be BL stars. This implies 91% observed occurrence rate, which is the highest value reported so far. The cumulative distribution function of the observed maximum side lobe amplitudes is shown in Fig. 5. We

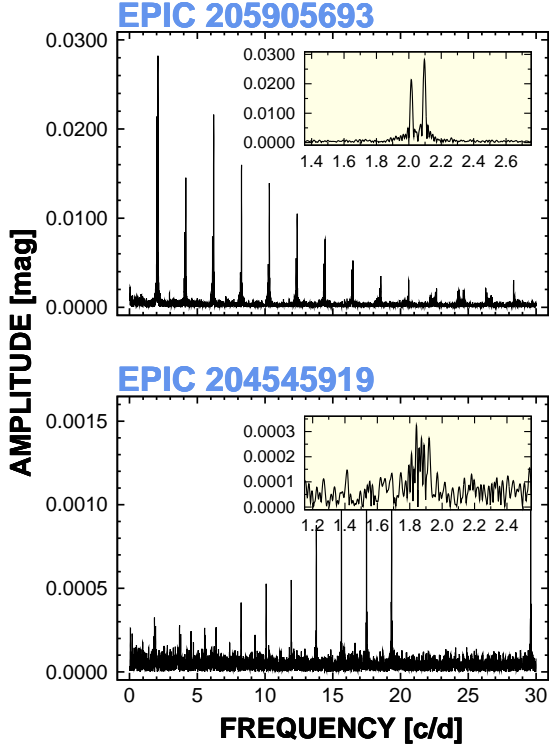


Fig. 4. Examples for high (upper panel) and low SNR (lower panel) detections. The amplitude spectra shown are the results of the DFT analysis of the TFA(FOUR) time series by using the fundamental pulsation frequencies and their first 14 harmonics both in the TFA filtering and in the pre-whitening. The peaks come either from the BL side lobes or from the high-frequency components leaked through the Nyquist frequency at ~ 24.47 c/d.

see that some 40% of the BL population originates from stars showing a rather small modulation, under 0.002 mag.² It is also observed that the CDF has a break at ~ 0.0015 mag, suggesting perhaps two different populations of BL stars (or maybe even three, if we consider the further break susceptible at the large $\{A_m\}$ limit of 0.03 mag). Because of the importance of the population with low $\{A_m\}$, in Fig. 6 we illustrate the actual observable light curve variations for two cases. Partially because of the long cadence of the data, in both cases the amplitude variations are not visible in the full-scale light curves. Therefore, we zoomed to the upper envelopes in the middle and lower panels.

4. The underlying rate

It is clear that the orders of magnitude difference between the accuracy of the MACHO and K2 data should be an important source of the stunning difference in the observed $\{A_m\}$ distributions. Here we test the effect of the observational noise on the derived occurrence rates.

Our testbase for the K2 data is the set of 151 RRab stars analyzed in this paper. For the MACHO data we use a larger set of non-BL (single period) RRab stars consisting of some 1700

² It is recalled that this is the size of the largest side lobe. Because additional components are frequently present, the total amplitude of the modulation is, in general, larger.

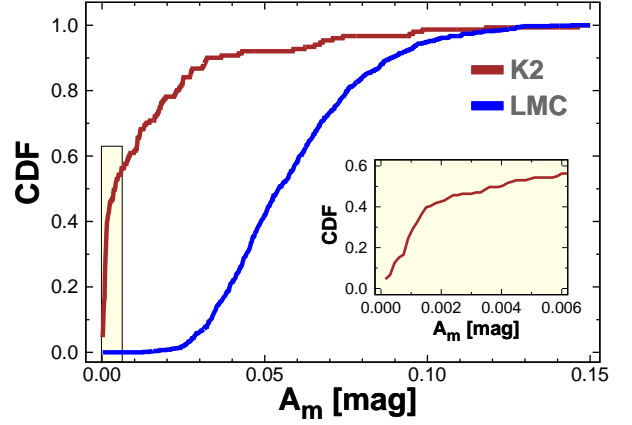


Fig. 5. Cumulative distribution function of the maximum side lobe amplitudes of the 138 BL stars identified in this work. For comparison, the same function is also shown for the 731 BL stars identified in the MACHO LMC sample by Alcock et al. (2003). The inset shows the blow-up of the region indicated in the main plot.

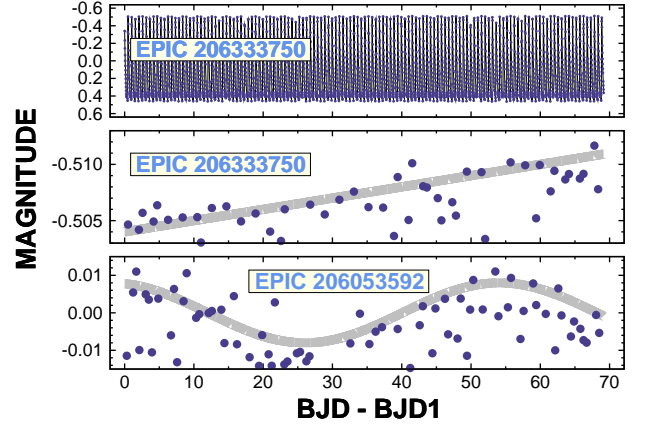


Fig. 6. Examples for small amplitude modulations from C03. *Uppermost panel:* light curve plotted on the scale of the full range of variation. *Middle panel:* zoom on the upper envelope. *Lower panel:* as in the middle panel, but for a star with a modulation period of 56 days. The gray lines are only for guiding the eyes in tracing the amplitude variation.

stars from our earlier analysis in Alcock et al. (2003).³ The tests constitutes of the following steps. First, with the aid of an *injected signal*⁴ analysis, we check the detection rates at various test amplitudes. We use six different amplitudes both for the K2 and for the MACHO data and save the result for the occurrence rate test. The range of amplitudes ensures that for each star we have at least one detection. The frequency of the injected signal is placed at $f_{inj} = 1.11f_0$. This choice yields a component at a relative unpopulated regime for the K2 data, which is important in avoiding interference with the signals already present in the data (for the MACHO data this is less of a problem, due

³ We aim at a larger statistical sample, therefore we employ the subset of the non-BL stars. By using the BL stars, we get the same result.

⁴ Importantly, we inject the test signal in the SAP data and proceed as with the real (observed) data. Injecting the test signal in the TFA-filtered data would falsify (i.e., increase) our detection rates, because of the considerable lower noise resulting from the filtering.

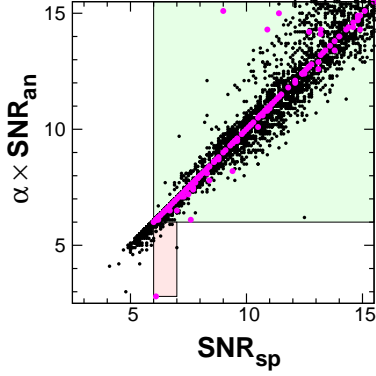


Fig. 7. Detected signal-to-noise ratios (SNR_{sp}) in the Fourier spectra vs the calibrated analytical signal-to-noise ratio SNR_{an} . Each star is characterized by its own calibration factor α and SNR_{an} . The calibration has been derived from injected signal tests, as described in the text. The MACHO and K2 stars are plotted by black and magenta, respectively. Pale green and red rectangles, respectively, denote the parameter regimes where the two SNR estimates yield consistent/inconsistent detection result.

to the high noise). The injected signal is labelled as “detected” if the corresponding SNR is greater than 6.0 and the distance of the associated peak from the injected value is less than $0.5/T$, where T is the total time span of the observations.

Because the estimation of the occurrence rate test requires the knowledge of the detection likelihood for any amplitude given by the distribution of $\{A_m\}$, we calibrate the test SNR values observed in the spectra (SNR_{sp}) with the analytical form of $SNR_{an} = A_{inj} \sqrt{N}/\sigma$ via a simple scaling factor α .⁵ Fig. 7 shows the result of this calibration. We see that except for a negligible small fraction of the test values we can tell reliably for each star if the injected signal were detectable or not.

Now we can use the *observed* $\{A_m\}$ distribution for the K2 data as shown in Fig. 5, and generate large number of amplitudes and check if they are detectable in the stars of the sample. The results are summarized in Table 2.

Table 2. Estimates on the observed occurrence rates

Method	R_{true}	K2	MACHO
observations	–	$91 \pm 2\%$	$12 \pm 0.4\%$
$\{A_m\}$ constraint: NO	100%	$83 \pm 3\%$	$14 \pm 1\%$
$\{A_m\}$ constraint: a	100%	$85 \pm 3\%$	$13 \pm 1\%$
$\{A_m\}$ constraint: b	100%	$91 \pm 2\%$	$14 \pm 1\%$
$\{A_m\}$ constraint: NO	90%	$74 \pm 3\%$	$13 \pm 1\%$
$\{A_m\}$ constraint: a	90%	$76 \pm 3\%$	$12 \pm 1\%$
$\{A_m\}$ constraint: b	90%	$81 \pm 3\%$	$12 \pm 1\%$

Notes:

- All tests have been made under the assumption that the true distribution of the maximum modulation side lobes $\{A_m\}$ follow the observed distribution as derived on the K2 data (see Fig. 5).
- The type of constraint employed in the distribution of $\{A_m\}$ is given by the letters *a* and *b*, corresponding to the regions indicated in Fig. 8.
- Statistical errors attached to the observed values are based on Alcock et al. (2003).

⁵ Because of the importance of the low-SNR regime, we weight heavily (proportionally to SNR_{sp}^{-6}) these values in the least squares fit for α .

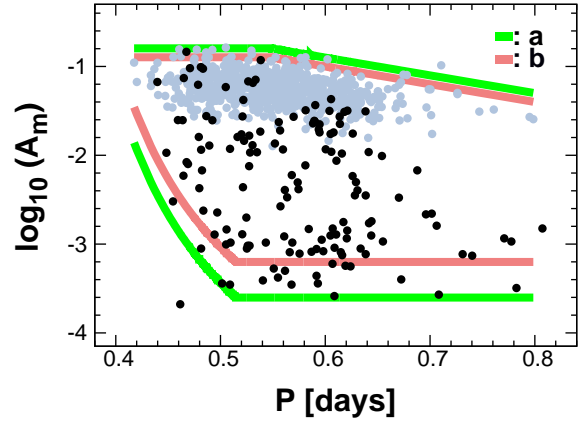


Fig. 8. Observed modulation amplitudes (Fourier amplitudes – in [mag] – of the largest sidelobes in the vicinity of the frequency of the fundamental mode) versus pulsation period. Black dots are for the K2 sample of this work, whereas pale ones are for the Blazhko stars from the MACHO survey of Alcock et al. (2003). The various bounds of the region denoted by *a* and *b* are used in the estimation of the underlying occurrence rates.

In the first row we show the observed rates. In the next three rows we assume 100% true occurrence rate, and impose various constraints on the injected signal amplitude. In the simplest case we assume that each star has equal probability to sample the full range of modulation amplitudes according to the observed distribution on the K2 dataset. This assumption leads to a significant underestimation of the observed K2 rate. An obvious guess for a possible source of the underestimation is that the (unknown) dependence of the BL phenomenon on the stellar parameters cuts out low amplitude modulations for specific parameter combinations. We tested this possibility by examining the period dependence of the modulation amplitudes. Fig. 8 shows that indeed, at short periods, we have an apparent lack of BL stars. Applying the constraints imposed by the lines labelled by *a*, we get an increase (see third row), but it is still insufficient to reproduce the observed rate for the K2 data. Shrinking further the allowed region (case *b*) we arrive to a nice match for the K2 data. We note that at this level we have no knowledge on the actual parameter space of the BL phenomenon. It might be more complicated than the one used here (i.e., a simple smooth amplitude cut). Therefore, the deeper cut seen in case *b* could be less severe as it might seem from the several outliers in Fig. 8 for this particular cut.

Because of the higher noise level of the MACHO data, they yield roughly the same, slightly discrepant value, independently of the restrictions posed on the modulation amplitude. It seems that the only way to reach the observed value is to decrease the underlying occurrence rate. Indeed, as shown in the last three rows, assuming 90% true rate yields the desired rate for the MACHO/LMC data. Unfortunately, the lower rate completely spoils the fine agreement for the K2 data. This may imply some real difference in the BL occurrence rates between the LMC and the Galactic field.

5. Conclusions

We analyzed 151 RR Lyrae stars from the K2 fields C01–C04, classified earlier by Armstrong et al. (2016) as fundamental mode (RRab) stars and searched for Blazhko variability, gen-

erally characterized as stars displaying close frequency components to that of the fundamental mode. Our analysis adapts the method used widespread in the field of transiting extrasolar planets to filter out systematics from ground- and space-based data. These systematics act as colored noise in the frequency analysis, and falsify the result for signals with amplitudes similar to those of the systematics. The modified method takes into consideration of the large amplitude component (stellar pulsation) of the RRab signal and maintains its shape with a simultaneous systematics filtering. Our analysis has led to the following results.

- We report an occurrence rate of 91% for the Blazhko phenomenon among the stars analyzed. This is the highest rate detected so far.
- After correcting for observational bias due to finite observational accuracy, we find that the underlying (true) rate should be very close to 100% in the part of the Galactic field covered by C01–C04.
- This high true rate is confirmed by a similar debiasing applied to the MACHO data on LMC (Alcock et al. 2003), although the optimum rate turned out to be closer to 90% for this dataset.
- The cumulative distribution function of the modulation side lobe amplitudes has a clear break at 0.0015 mag, leading to a conjecture on the possibility of the existence of a different subclass of Blazhko stars at small modulation amplitudes.
- Because of the very common nature of the Blazhko phenomenon, it seems likely that ideas employing radial mode resonances will face difficulties in explaining this level of commonality.

Acknowledgements. I thank to David Armstrong for a quick reply to my inquiry on the data availability. I also appreciate the information given on the analysis of the WASP data by Paul Greer. Special thanks are due to Eric Petigura for making the K2 time series data available to the community in simple format through the IPAC ExoFOP site. This research has made use of the NASA Exoplanet Archive, which is operated by the California Institute of Technology, under contract with the National Aeronautics and Space Administration under the Exoplanet Exploration Program.

References

- Aigrain, S., Parviainen, H., & Pope, B. J. S. 2016, MNRAS, 459, 2408
 Alcock, C., Alves, D. R., Becker, A., et al. 2003, ApJ, 598, 597
 Angus, R., Foreman-Mackey, D., & Johnson, J. A. 2016, ApJ, 818, 109
 Armstrong, D. J., Kirk, J., Lam, K. W. F. et al. 2016, MNRAS, 456, 2260
 Benkő, J. M., Plachy, E., Szabó, R. et al. 2014, ApJS, 213, 31
 Blazhko, S. 1907, Astr. Nachr., 175, 325
 Christy, R. F. 1964, Rev. Mod. Phys. 36, 555
 Foreman-Mackey, D., Montet, B. T., Hogg, D. W. et al., 2015, ApJ, 806, 215
 Buchler, J. R. & Kolláth, Z. 2011, ApJ, 731, 24
 Jurcsik, J., Sódor, Á., Szeidl, B., et al. 2009, MNRAS, 400, 1006
 Kovacs, G., Bakos, G., & Noyes, R. W. 2005, MNRAS, 356, 557
 Kovacs, G. & Bakos, G. A. 2008, CoAst, 157, 82
 Kovacs, G., Hartman, J. D., Bakos, G. A. et al. 2014, MNRAS, 442, 2081
 Kovacs, G. 2016, CoKon, 105, 61
 Kovacs, G., Hartman, J. D., & Bakos, G. A. 2016, A&A, 585, 57
 Kovacs, G. 2018, to appear in Proc. Polish Astron. Soc. (arXiv:1804.01894)
 Petigura, E. A., Schlieder, J. E., Crossfield, I. J. M., et al. 2015, ApJ, 811, 102
 Plachy, E., Klagyivik, P., Molnár, L. et al. 2017, EPJ Web of Conf., Vol. 160, id.04009
 Shapley, H. 1916, ApJ, 43, 217
 Szabó, R., Benkő, J. M., Paparó, M. 2014, A&A, 570, 100
 Smith, J. C., Stumpe, M. C., Van Cleve, J. E. et al. 2012, PASP, 124, 1000
 Smolec, R. 2016, Proc. of the Polish Astron. Soc, Vol. 3, pp. 22
 Tamuz, O., Mazeh, T., & Zucker, S. 2005, MNRAS, 356, 1466